J. Non-Newtonian Fluid Mech. 165 (2010) 1505–1515

Contents lists available at ScienceDirect

Journal of Non-Newtonian Fluid Mechanics

journal homepage: www.elsevier.com/locate/jnnfm

Flow of wormlike micelle solutions past a confined circular cylinder

Geoffrey R. Moss, Jonathan P. Rothstein*

Department of Mechanical and Industrial Engineering, University of Massachusetts, Amherst, MA 01003, USA

ARTICLE INFO

Article history:
Received 8 September 2009
Received in revised form 1 July 2010
Accepted 29 July 2010

Keywords:
Circular cylinders
Wormlike micelle solution
Viscoelastic
Extensional flow

ABSTRACT

In this paper, we present the results of an investigation into the flow of a series of viscoelastic wormlike micelle solutions past a confined circular cylinder. Although this benchmark flow has been studied in great detail for polymer solutions, this paper reports the first experiments to use a viscoelastic wormlike micelle solution as the test fluid. The flow kinematics, stability and pressure drop were examined for two different wormlike micelle solutions over a wide range of Deborah numbers and cylinder to channel aspect ratios. A combination of particle image velocimetry and pressure drop measurements were used to characterize the flow kinematics, while flow-induced birefringence measurements were used to measure the micelle deformation and alignment in the flow. The pressure drop was found to decrease initially due to the shear thinning of the test fluid before increasing at higher flow rates as elastic effects begin to dominate the flow. Above a critical Deborah number, an elastic instability was observed for just one of the test fluids studied, the other remained stable for all Deborah number tested. Flow-induced birefringence and velocimetry measurements showed that observed instability originates in the extensional flow in the wake of the cylinder and appears not as periodic counter-rotating vortices as has been observed in the flow of polymer solutions past circular cylinders, but as a chaotic rupture event in the wake of the cylinder that propagates axially along the cylinder. Reducing the cylinder to channel aspect ratio and the degree of shearing introduced by the channel walls had a weak impact on the stability of the flow. These measurements, when taken in conjunction with previous work on flow of wormlike micelle solutions through a periodic array of cylinders, definitively show that the instability can be attributed to a breakdown of the wormlike micelle solutions in the extensional flow in the wake of the cylinder.

1. Introduction

The flow of viscoelastic fluids past a submerged body such as a sphere or a cylinder is an academically and industrially important class of flow problems which has received significant amount of attention over the last few decades [1–3]. The common feature of all these flows are stagnation points at the leading and trailing edge of the submerged body which can lead to long residence times and large deformation of the polymers or wormlike micelles in the fluids. For polymer solutions, the strong extensional flow in the wake of circular cylinders has been shown to distort the Newtonian velocity profile [4–6], produce significant elastic stress [7] and result in an elastic instability [3,8,9]. In industrial applications, the onset of elastic instabilities can be the limiting factor for production and quality control processes, making a better physical understanding of the conditions necessary for onset of the instability essential for a broad spectrum of commercially relevant viscoelastic fluids.

The flow of a viscoelastic polymer solution past a single circular cylinder is a classically studied problem [3,4,7,9–17] with both experimental, analytical and numerical approaches. There are a number of reasons for such a breadth and depth of literature on the subject. First, as seen in Fig. 1, the flow upstream and far downstream of the cylinder is Poiseuille while the flow around the cylinder is complex, containing regions of shear in the gap between the cylinder and the bounding wall and extensional flow downstream of the cylinder. The relative strength of, and interplay between these regions can be easily modified by changing the aspect ratio of the cylinder to channel height [3]. Secondly, there are no geometric singularities such as those present at the corners of a contraction flow [18]. This flow thus lends itself particularly well to numerical studies as much of the meshing and simulation complexity is abated by the absence of a singularity. Finally, there exists an analytic solution to the kinematics of Newtonian flow past a circular cylinder at low Reynolds and Deborah number to compare numerical simulations and experimental results against [5,6]. The Reynolds number is defined as $Re = \rho UR/\eta$ and the Deborah number is defined as $De = \lambda/\tau$. Here U is the average velocity in the channel, R is the cylinder radius, ρ is the fluid density, λ is the characteristic relaxation time of the fluid, η is the kinematic viscosity, and $\tau = R/U$ is the residence time of the polymer near the cylinder which is often equivalent to the inverse shear rate, $\dot{\gamma}$.

* Corresponding author.

0377-0257/$ – see front matter © 2010 Elsevier B.V. All rights reserved.
doi:10.1016/j.jnnfm.2010.07.014

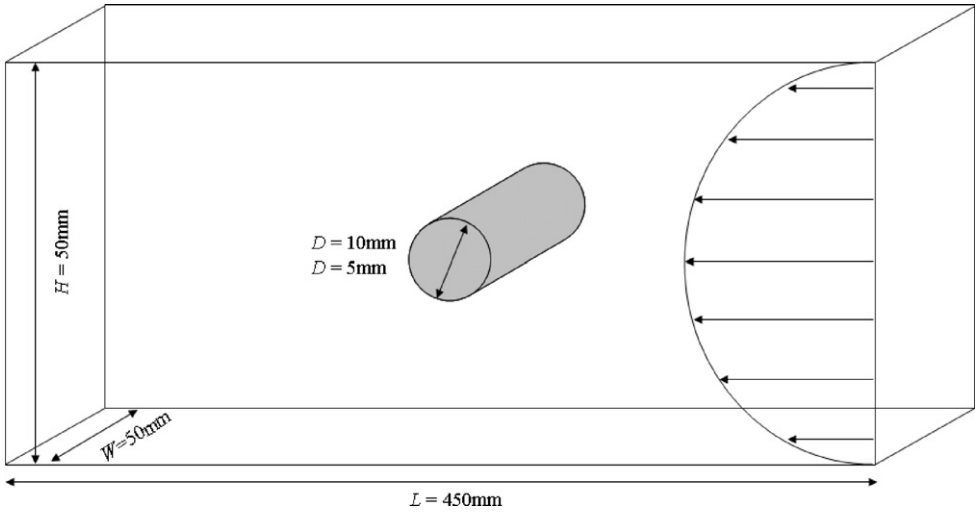

Fig. 1. Schematic diagram of circular cylinder used in the experimental flow cell.

An excellent, in-depth review of the older literature is presented in McKinley et al. [3]. We will not attempt to duplicate their work here, but rather focus on some of the more recent developments and emphasize the recent work done with surfactant solutions. In order to simulate the flow numerically, the governing equations of motion must be coupled with a constitutive model for the equation of state, relating stress and deformation. In a numerical investigation of the flow of viscoelastic fluids past a cylinder, Hulsen et al. [14] used both Oldroyd-B and Giesekus equations of state to observe the response of the drag coefficient to varying flow conditions. Over the range of Deborah numbers tested, they found that the dimensionless drag coefficient was not only time variant, but was a non-linear function of Deborah number. Their results show that the drag coefficient initially decreases with increasing Deborah number, then exhibits an inflection point and begin to increase with increasing Deborah number. More recently, Oliveira and Miranda [19] performed a numerical study employing a FENE-CR model to investigate the nature of the instability in the wake of a cylinder. Similar trends in pressure drop were observed between the two studies, as well the onset of an elastic instability. Their results show that in flows where the local Deborah number exceeds $De = \lambda\dot{\gamma} \approx 1.3$ a time-dependant drag coefficient emerges. These simulation results agree well with experimental measurements.

Fluid flow around a cylinder has also been the subject of much experimental treatment. Both McKinley et al. [3] and Baaijens et al. [10] used laser Doppler velocimetry measurements to observe the behavior and flow patterns generated by a highly elastic polyisobutylene (PIB) Boger fluids flowing around a circular cylinder. Their velocity profile measurements showed a parabolic profile upstream which flattened as the fluid approached the cylinder, developing off-center maxima as the fluid approaches within a diameter of the cylinder. The influence of the cylinder was found to persist several diameters downstream. At low Deborah numbers, the velocity profile is fore-aft symmetric, however, as the Deborah number is increased the symmetry is broken and the influence of the cylinder relaxes away more slowly, extending further downstream. Baaijens et al. [20] showed that the extensional flow in the wake of the cylinder resulted in a strong birefringent tail that could extend up to ten radii downstream. McKinley et al. [3] observed an instability in the wake of a single cylinder lying perpendicular to the bulk flow above a critical Deborah number of $De_{crit} = 1.3$ for a cylinder to channel aspect ratio of $\beta = D/H = 0.5$. Above this critical Deborah number, a three-dimensional flow was observed isolated to the wake of the cylinder with stationary vortices spaced periodically along the axis of the cylinder. The wavelength of these cells was found to scale roughly with the cylinder diameter. These observations were later confirmed and extended by Shiang et al. [9] through high-resolution particle image velocimetry (PIV) measurements. Changing the aspect ratio had only a small effect on the critical Deborah number, suggesting that it is the extensional flow in the wake of the cylinder and not the shear flow around the cylinder that causes the flow instability [3].

There are many other experimental studies in the canon of investigations into the flow of viscoelastic polymer solutions around a cylinder; however, no experiments to date have investigated the flow of viscoelastic surfactant solutions past a single cylinder. A recent study did, however, investigate the flow of wormlike micelle solutions past a periodic array of cylinders [21] and will be discussed in some detail. Surfactants are amphiphilic molecules which have both a bulky hydrophilic head and a relatively short hydrophobic tail. Above their critical micelle concentration (CMC), surfactant molecules in water will spontaneously self-assemble into large aggregates known as micelles to minimize the exposure of their tails to water [22–24]. There have been a number of studies investigating the flow of dilute surfactant solutions, just above their CMC, past single cylinders at high Reynolds numbers [25,26]. At these low concentrations, the surfactant solutions for short unentangled rods which demonstrate little to no elasticity and a modest amount of shear thinning, but have been shown to reduce drag in turbulent pipe flows [27]. For the flow past a cylinder, the addition of surfactant was found to reduce intensity of the turbulent fluctuations in the wake of the cylinder and reduce the overall drag on the cylinder [25,26].

In this work, we focus on viscoelastic wormlike micelles [22,28], which, as suggested by their pseudonym, 'living polymers,' display many of the same viscoelastic properties of polymers. However, although both wormlike micelle solutions and polymer solutions can be viscoelastic, wormlike micelles are physically very different from polymers. Whereas the backbone of a polymer is covalently bonded and rigid, wormlike micelles are held together by relatively weak physical attractions and as a result are continuously breaking and reforming with time. In an entangled network, both individual polymer chains and wormlike micelles can relieve stress through reptation driven by Brownian motion [23]. However, unlike polymeric fluids, wormlike micelle solutions have access to a number of stress relief mechanisms in addition to reptation. Wormlike micelles can relieve stress and eliminate entanglement points by either breaking and reforming in a lower stress state [24] or alternatively by creating a temporary branch point which allows

two entangled micelles to pull right through each other thereby eliminating the entanglement point and relieving stress in what has become known as a 'ghost-like' crossing [29]. Additionally, the constant re-organization of the network structure results in several interesting phenomenon when subjected to strong extensional flows.

Shear and extensional rheological measurements of wormlike micelles have shown these viscoelastic solutions to be heavily shear thinning [24] and extensionally strain hardening [30]; however, these are just a small subset of the wealth of behaviors that make such solutions interesting. Under shear, wormlike micellar solutions can demonstrate shear banding [31]. In filament stretching extensional rheology measurements, when a filament of a wormlike micelle solution had experienced a large enough stress and strain, it has been found to rupture near its axial mid plane [30,32]. This behavior has been observed most recently by Bhardwaj et al. [32], and is believed to be caused by a scission of individual micelle chains due to extensional stresses built up in the flow. This failure can manifest itself as a new class of flow instabilities which are present in both pure extensional flows, and complex flows as well. Take for example the flow around a sphere, the kinematics of which are very similar to the flow around a cylinder presented here. This flow contains regions of shear around the circumference of the sphere, along with regions of extension in the wake of the sphere. Above a critical sedimentation rate, spheres falling through a wormlike micelle solution were recently shown to exhibit a new class of elastic instabilities in the wake of a sphere [33,34]. By measuring the flow fields with particle image velocimetry (PIV) and flow-induced birefringence (FIB) Chen and Rothstein [33] were able to explore the kinematics of the flow and directly relate this flow instability to the rupture of these micellar solutions during filament stretching.

More recently, Moss and Rothstein [21] observed a similar instability in the flow of a series of wormlike micelle solutions around a periodic array of circular cylinders. They were able to directly correlate the measurements of pressure drop, PIV, and FIB to the extensional and shear rheology of the test fluids. Measurements of pressure drop as a function of the Deborah number were found to initially decrease due to the shear thinning of the fluids, followed by an increase with increasing Deborah number due to the extensional thickening. One of the fluids, a solution of cetyltrimethyl ammonium bromide (CTAB) and sodium salicilate (NaSal) was observed to exhibit a flow instability above a critical Deborah number, while the other solution of cetylpyridinium chloride (CPyCl) and NaSal remained stable for all Deborah numbers tested. It was found that although both fluids strain hardened and ruptured in the homogeneous extensional flow imposed by a filament stretching rheometer, the CTAB/NaSal solution did so at an accumulated strain of $\varepsilon = 2.5$, while the CPyCl/NaSal solution requires an accumulated strain of $\varepsilon = 3.3$ to fail. By making measurements of the extension rate and strain accumulated in the wake of the circular cylinders it was found that the strain approached a value of $\varepsilon = 2.5$. At the higher Deborah numbers tested, the rate of strain was enough to induce rupture in the CTAB/NaSal solutions, but not the CPyCl/NaSal solutions.

The single circular cylinder is essentially a periodic array of cylinders spaced infinitely far apart. In such flow geometry, the extensional flow in the wake of the cylinder is never in competition with the compressive flow at the stagnation point in the front of the 'next' cylinder. Additionally and more importantly, the importance of the shear flow produced by the channel walls can be minimized by working with single cylinder having a small cylinder to channel aspect ratio. Thus the single cylinder geometry allows for a conclusive study of the effect of the extensional flow on the stability of viscoelastic wormlike micelle solutions. Finally, although there are many similar studies utilizing polymer solutions, this work is the first to investigate the flow of viscoelastic wormlike micelle solution past confined circular cylinders.

The outline of this paper is as follows. In Section 2, we briefly describe the experimental setup, the implementation of several measurement techniques including flow-induced birefringence and particle image velocimetry and the shear and extensional rheology of the wormlike micelle solutions used. In Section 3 we discuss the experimental results and in Section 4 we conclude.

2. Experimental setup

2.1. Flow geometry and experimental setup

A schematic diagram of the test geometry can be seen in Fig. 1. The circular cylinders were fabricated from acrylic rod, and precisely lathed down to uniform diameters of $D = 10$ mm and $D = 5$ mm. The cylinders were mounted transversally at the center of a rectangular channel with a cross-sectional area of 50 mm square and a length of 450 mm. This length was chosen to insure that the fluid had a residence time of at least 10 times the relaxation time from the time it entered the flow cell to the time in reached the cylinder so that it could reach steady state even at the highest Deborah numbers. In order to study containment effects and explore the interactions between the flow near the cylinder and the channel walls, the blockage ratio was varied from 1:5 to 1:10 by varying the diameter of the cylinder.

A positive displacement piston pump was employed to minimize any driving pressure fluctuations. The piston motion was controlled with addressable micro-staging (Parker Industries), capable of a flow rate resolution of 4 mm^3/s. The flow cell was plumbed to the piston using 25 mm inner diameter tubing and a diffuser/nozzle was used at the entrance and exit of the flow cell to minimize entrance effects. In this study, the Deborah number was varied over two decades between $0.1 \leq De = \lambda U/R \leq 10$ in order to explore the pressure drop, flow kinematics, and flow-induced birefringence of two different solutions of wormlike micelles at two different blockage ratios. Details of the PIV and FIB techniques employed here can be found in Ref. [21]. The Deborah Number, was evaluated using the average velocity, U, evaluated at the point of maximum blockage in the channel. The Deborah number characterizes the strength of the extensional flow in the wake of the cylinder. Alternatively, a Weissenberg number, $Wi = \lambda\dot{\gamma} = \lambda U/(H - D)$, can be introduced to characterize the strength of the shear flow in the channel.

In order to measure the deviation from a Newtonian fluid behavior, the flow cell was constructed with pressure taps machined flush with the bounding side plates at positions 5 cm upstream and downstream of the circular cylinder. Pressure lines were then plumbed from the taps into a differential pressure transducer (Omega PX154010-DI) having a range from 0 to 250 Pa. The signal was then fed into a data acquisition board and sampled at 100 Hz using a custom written Labview VI.

2.2. Sample preparation

Wormlike micelle solutions assembled from two different surfactant/salt combinations were chosen for this study. The first set of wormlike micelle solutions that were tested were made up 100 mM of the cationic surfactant CPyCl (Fisher Scientific) and 50 mM of NaSal (Fisher Scientific) dissolved in a brine of 100 mM NaCl in distilled water. The second test fluid was composed of 50 mM of another cationic surfactant CTAB (Fisher Scientific) and 50 mM of NaSal in deionized water. The surfactants and salts were dissolved in water on a hot plate with a magnetic stirring bar. During mixing, a moderately elevated temperature was applied to reduce viscosity

Table 1
Parameters characterizing the rheology of the wormlike micelle solutions at $T = 25\,^{\circ}C$.

			CPyCl/NaSal 100 mM/50 mM	CTAB/NaSal 50 mM/50 mM
Zero-shear viscosity	η_0	[Pa-s]	11	62
Plateau modulus	G_0	[Pa]	27	10.9
Relaxation time	λ	[s]	0.50	5.7

and aid in uniform mixing. After the solutions were fully dissolved, they were allowed to settle at room temperature for at least 24 h before any experiments were performed to allow air bubbles introduced during mixing to rise out of solution. At the concentrations used, the wormlike micelle solutions are concentrated with a significant number of entanglement points per chain [22].

2.3. Rheology

A complete set of steady and dynamic shear rheology data for each of the wormlike micelle solutions used in this study can be found in Moss and Rothstein [21]. In each case, the linear viscoelastic response of the wormlike micelle solutions is well fit by the predictions of a single mode Maxwell fluid. For completeness, the viscoelastic properties of the fluids including zero-shear-rate viscosity, η_0, relaxation time, λ, and the elastic plateau modulus, G_0, are listed in Table 1. As described in Ref. [21], the steady shear rheology is more complex. At low shear rates, the viscosity is constant, however, at moderate the shear rates, the fluids shear thin. The rate of shear thinning increases with increasing shear rate eventually approaching a slope of $\eta \propto \dot{\gamma}^{-1}$. At these large shear rates, the fluids have been shown to shear band [35], although as we will discuss in the following sections, no shear banding was observed in our experiments.

These particular solutions of wormlike micelles have been the subject of many extensional rheology studies in recent years [30,32,36,37]. However, for completeness and for the purpose of enabling a discussion on the differences observed in the response of the two wormlike micelle solutions in the flow tested here, a representative set of transient extensional rheology data from our filament stretching extensional rheometer is reproduced here in Fig. 2. In Fig. 2, the Trouton ratio, $Tr = \eta_E/\eta_0$, of the 50/50 mM CTAB/NaSal and 100/50 mM CPyCl/NaSal wormlike micelle solutions is plotted as a function of total accumulated Hencky strain for a Deborah numbers of $De = 1.3$. The extensional viscosity, η_E, of both fluids was found to increase monotonically with increasing Hencky strain and demonstrate reasonably strong strain hardening. The important point to take away from Fig. 2, is that although the CPyCl/NaSal solution was found to strain harden more than the CTAB/NaSal solution, the CTAB/NaSal solution strain hardened much more quickly, achieving maximum extensional viscosity at $\varepsilon \cong 2.5$, as opposed to $\varepsilon \cong 3.3$. In both cases, the filament stretching experiment ended before a steady-state value of the extensional viscosity could be reached because the fluid filament ruptured near the axial midplane. It has been hypothesized that the tensile stress of rupture corresponds to the maximum stress that the micelles can withstand before they begin to fail en masse [30]. For the CPyCl/NaSal solution, the tensile stress at rupture was found to be $\Delta\tau_E \cong 8500$ Pa while for the CTAB/NaSal solution tensile stress at rupture was found to be lower at about $\Delta\tau_E \cong 2500$ Pa. In both cases, the stress at rupture was found to be independent of extension rate [30]. The dynamics of the filament rupture have been captured with high-speed photography in the past and the interested reader is referred to Chen and Rothstein [33] or Bhardwaj et al. [32] for details. We will see in the following sections that the extensional rheology differences between these two wormlike micelle solutions has a significant effect on the response of these fluids as they flow past a circular cylinder.

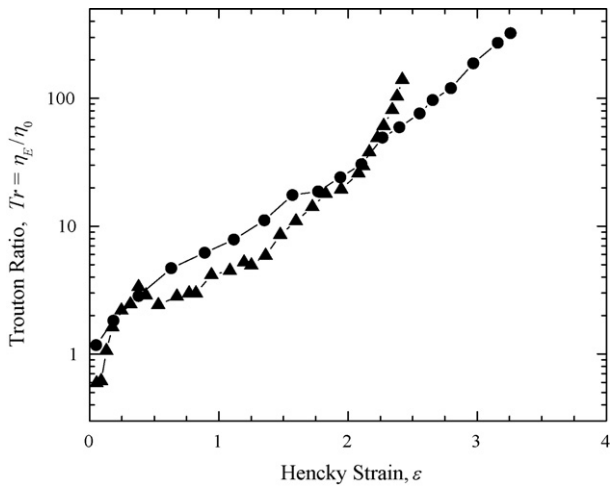

Fig. 2. Transient extensional rheology for the 50/50 mM CTAB/NaSal wormlike micelle solution '▲' and the 100/50 mM CPyCl/NaSal wormlike micelle solution '●', both stretched at a Deborah number of $De_{ext} = 1.3$. The figure shows the evolution of the Trouton ratio, $Tr = \eta_E/\eta_0$, as a function total accumulated Hencky strain. Both experiments end with the rupture of the fluid filament before a steady-state extensional viscosity could be reached.

When analyzing and presenting the experimental data, the relaxation times and viscosities were adjusted to their values at a reference temperature of $T_{ref} = 25\,^{\circ}C$ using time–temperature superposition with a shift factor, a_T, defined by the Arrhenius equation [38]. Within the temperature range of our experiments the Arrhenius form of the time-temperature superposition shift factor was found to be in good agreement with the rheological data for each of the wormlike micelle solutions tested. However, because of the sensitivity of the underlying wormlike micelle structures to changes in temperature, every effort was made to maintain the fluid temperature to within plus or minus a few tenths of a degree of $T = 25\,^{\circ}C$ for all of the experiments presented herein. This also guaranteed that all of the experiments were performed above the Krafft temperature which is just below room temperature for each of the surfactants used.

3. Results

3.1. Pressure drop measurements

The pressure drop across the cylinder was measured as a function of Deborah number, micellar solution and blockage ratio of the channel. For all of the experiments presented here, the large viscosity of the solutions, lead to a vanishingly small Reynolds number, $Re < 10^{-3}$. The time-averaged pressure drop is presented in Fig. 3 for both micelle solutions in both the 1:5 and 1:10 blockage ratio channel. In Fig. 3, a dimensionless pressure drop is presented where the measured pressure drop is normalized by the response of a Newtonian fluid with the same zero-shear viscosity:

$$\Pi \equiv \frac{\Delta P_{measured}}{\Delta P_{Newtonian}}. \quad (1)$$

Since no analytic solution for a Newtonian fluid through our flow geometry exists, the low-Deborah number pressure drop ($De << 1$), which increases linearly with increasing flow rate, was used to approximate the Newtonian response and normalize the pressure drop data in Eq. (1) [18,21]. A solution does, however, exist for the flow past an infinitely long circular cylinder between two infinite plates [5].

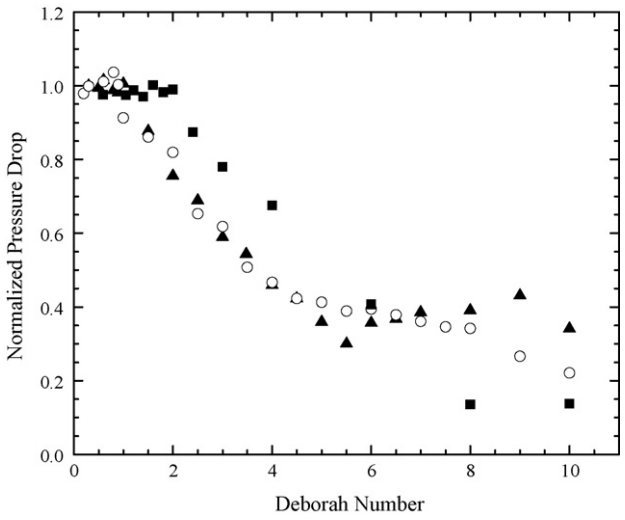

Fig. 3. Normalized pressure drop as a function of Deborah number for the flow past a circular cylinder of the CTAB/NaSal solution at a blockage ratio of 1:5 (▲) and 1:10 (■), and the CPyCl/NaSal solution at a blockage ratio of 1:5 (◯).

The normalized pressure drop curve seen in Fig. 3 was found to exhibit four distinct regimes. In the low-Deborah-number regime, the normalized pressure drop is constant at essentially $\Pi \cong 1$. Although the zero-shear viscosities of the two solutions differ by a factor of approximately three and the characteristic relaxation times differ by a factor of almost five, when the flow in the 1:5 channel is cast in terms of Deborah number and pressure drop is measured at low to moderate Deborah numbers, the resulting plots are nearly identical. At a Deborah number greater than $De > 1$, where the bulk flow deforms the micelles faster than they can relax, a deviation in the pressure drop from a Newtonian response is observed. At moderate Deborah numbers ($1 < De < 4$), the normalized pressure drop decreases monotonically, with a slope of approximately $\Pi \propto De^{-2/3}$ with increasing Deborah number as a result primarily of the shear thinning of the micelle solutions. For the flow of a power-law fluid through a channel, the dimensionless pressure drop should go as $\Pi \propto De^{1-n}$ where n is the power-law exponent [38]. This is consistent with the expectation for a shear-thinning fluid like the CPyCl/NaSal solution which has a power-law exponent of approximately $n \approx 1/3$ over this range of shear rates. This observation demonstrates that, in this regime, the trends in pressure drop for the CPyCl/NaSal solution are due almost entirely to the flow in the bounding channel. However, the viscosity of the CTAB/NaSal solution shear thins more heavily, approaching a value of approximately $n \approx 0$ soon after the onset of shear thinning [21]. One would therefore expect a much steeper drop in pressure with Deborah number. This observation indicates that the presence of the cylinder and the extensional thickening of the fluid in the wake of the circular cylinder are offsetting some of the reduction in pressure drop due to shear thinning in the channel. The strength of the extensional flow in the wake of the cylinder, especially the CTAB/NaSal solution, will become more obvious when the full-field flow-induced birefringence images are presented in the next section. As the flow rate is increased further ($4 < De < 7$), the normalized pressure drop plateaus at about $\Pi \simeq 0.4$. In this regime, the solutions are both shear thinning as well as extensional thickening and the competition between these two effects roughly offset each other. At high Deborah numbers, a slight change in slope becomes apparent after the onset of a flow instability in the case of the CTAB/NaSal solution. The CPyCl/NaSal solutions were found to remain stable for all the experiments presented here and did not show the same magnitude of upturn in pressure drop as was observed in the case of a periodic array of cylinders [21]. These pressure drop trends are consistent with both experimental measurements [39] and numerical simulations of the flow of viscoelastic polymeric fluids past a single circular cylinder [7,20,40] as well as recent measurements of flow of wormlike micelle solutions past a periodic array of cylinders [21].

The effect of blockage ratio on the steady-state pressure drop is also shown in Fig. 3. In comparing the response of the two fluids to the varying blockage ratio, it is apparent that for the 1:10 ratio, the onset of shear thinning is pushed off until a Deborah number of $De = 2$, or twice that for the 1:5 ratio. If, however, the data were plotted as a function of Weissenberg number the data overlap nicely. This observation suggests that the decrease in pressure drop is primarily the result of shear thinning in the bounding channel and not caused by the shear flow around the circular cylinder. Additionally, the increased importance of the shear flow at lower blockage ratios results in a reduction of the high Deborah number limiting value of the dimensionless pressure drop which for the 1:10 case is approximately half of the 1:5 case. One of the reasons for testing two different blockage ratios was to try to determine if the flow instability was driven by the extensional flow in the wake of the cylinder or if the shear flow introduced by the bounding channel was critical for the flow to become unstable. In the case of the CTAB/NaSal solution, above a Deborah number $De > 4.5$ for the 1:5 blockage ratio and above $De > 6$ for the 1:10 blockage ratio, the pressure drop measurements were observed to fluctuate in time with an amplitude that increased with increasing Deborah number. The fluctuations did not appear to be time-periodic and fast Fourier transforms of the signal did not produce a clean fundamental frequency, rather the fluctuations appeared to be chaotic. If the instability resulted solely from the shear flow, one would expect that the critical value of the Deborah number for the onset of the instability in the 1:10 case would be precisely twice the value of the 1:5 case. Additionally, as the blockage ratio is reduced, the extensional deformation of the micelles in the contraction flow between the cylinder and the wall is reduced. Taken together, these observations provide convincing evidence that the origin of the instability is in the extensional flow in the wake of the cylinder and that the shear flow along the flow cell wall does not significantly affect the flow stability. Similar conclusions were hypothesized, but could not be rigorously shown in the flow through a periodic array of cylinders because of the complex interaction of the flow past multiple cylinders and the bounding flow cell [21]. The modest increase in critical Deborah number with decreasing blockage ratio is consistent with the observations of the elastic instability in the wake of cylinders where the test fluid was a viscoelastic polymer solution although we will see in the following sections that the form of the instability is very different. In the work of McKinley et al. [3], the critical Deborah number was found to increase by approximately 50% when the blockage ratio was halved.

3.2. Flow-induced birefringence (FIB)

Full-field flow-induced birefringence measurements were made using the crossed polarizer technique described in Ref. [21] for both wormlike micelle solutions and blockage ratios, and a series of Deborah numbers in each of the distinct flow regimes described in the previous section. The areas of large micellar deformation are clearly seen in Fig. 4 for the CPyCl/NaSal solution at a Deborah number of $De = 2.0$. In the case of the polarizers oriented at 0° and 90°, the regions of deformation due to shear are highlighted, and appear as relatively light areas or fringes. This can be seen clearly at 45° relative to the stagnation point in the front of the circular cylinder and along the channel walls. In the case of the polarizers oriented at 45° and 135°, the regions of extensional deformation are highlighted. It is known that in flows with stagnation points, that that a narrow region of high polymer or micelle deformation known

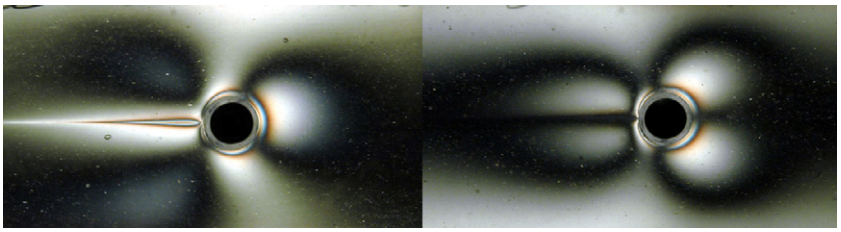

Fig. 4. Full-field flow-induced birefringence measurements of CPyCl/Nasal at a Deborah number of $De = 2$. In the left image, the crossed polarizers are oriented at 45° and −45° from the flow direction to highlight the regions of extensional deformation while in the right-hand image the crossed polarizers are oriented at 0° and 90° to highlight shear. The flow is from right to left.

as birefringent strands can form in the strong extensional flow just downstream of the stagnation point [41,42]. These birefringent strands appear as bright areas or fringes directly in the wake of the cylinder and at the stagnation point in the front of the cylinder in Fig. 4. These fringe patterns are in excellent qualitative agreement with the patterns observed in both experiments [20] and numerical simulations [7,40]. For the purpose of brevity, the discussion and figures that follow will focus on images taken with the polarizers at 45° and 135° in order to highlight extensional deformation of the wormlike micelle solutions because these images contain most of the pertinent information.

In Fig. 5, the birefringence patterns of the CTAB/NaSal solution and the CPyCl/NaSal solution for the 1:5 blockage ratio are compared over a range of Deborah numbers, while in Fig. 6, the birefringence patterns for the CTAB/NaSal solutions at the two blockage ratios are compared. An initial observation is that the CTAB/NaSal is considerably more birefringent for flows at comparable Deborah numbers. Even taking into account the difference in the stress-optical coefficient, it is clear that the CTAB/NaSal solution experiences considerably more extensional deformation at a given Deborah number. The birefringent patterns in Fig. 5 grow and scale with the Deborah number; both the extensional and shear patterns extend further away from the cylinder as the Deborah number is increased. The extensional tail in the wake of the cylinder grows dramatically at moderate Deborah numbers, extending five to ten cylinder diameters downstream. It is the growth in the strength of the extensional flow coupled with the extensional thickening of these wormlike micelle solutions that results in the plateau and eventual upturn in the dimensionless pressure drop presented in Fig. 3.

In both Figs. 5 and 6, the birefringence goes through several orders, indicating a substantial amount of deformation and thus stress accumulated by the fluid as it flows past the circular cylinder. Degree of deformation is found to increase with increasing Deborah number for both fluids and blockage rations. In comparing the two solutions in Fig. 5, we observe that the birefringent tail of the CTAB/NaSal solution (left) not only grows in length, but in width as well. It begins to dominate the flow field at higher Deborah numbers. For example, the illuminated region in the wake of the cylinder at a Deborah number of $De = 0.5$ extends approximately two diameters downstream. By doubling the Deborah number to $De = 1$, the tail goes through an order indicated by the fringe pattern and grows to approximately three diameters downstream. By further increasing the Deborah number to $De = 4$, the tail goes through several orders, extends over ten diameters downstream and grows in the spanwise direction to approximately three diameters. At this point, due to its spanwise growth, the confinement effects of the bounding channel begin to interact with the deformation field around the cylinder. In the case of the CPyCl/NaSal, the birefringent tail can be seen to go through orders and increase in downstream length as the Deborah number is increased, but does not appreciably grow in the spanwise direction. Further, the compressive region at the stagnation point in the front of the cylinder can be seen to go through far fewer orders in the case of the CPyCl/NaSal

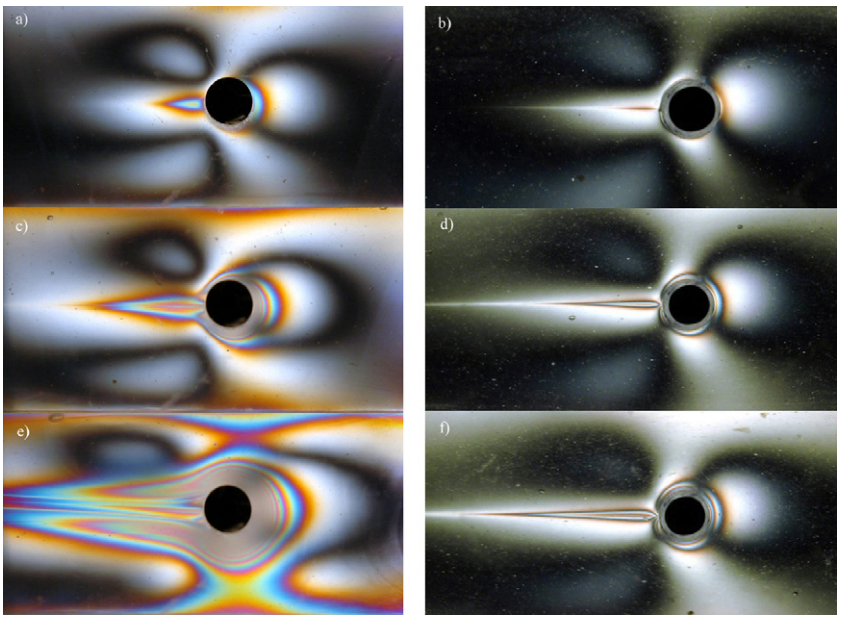

Fig. 5. The extensional birefringent patterns produced by setting the crossed polarizers at 45° and 135° for both the CTAB/NaSal solution (left) and the CPyCl/NaSal solution (right) at Deborah numbers of $De = 1.0$ (a and b), $De = 2.0$ (c and d), and $De = 4.0$ (e and f). The flow is from right to left.

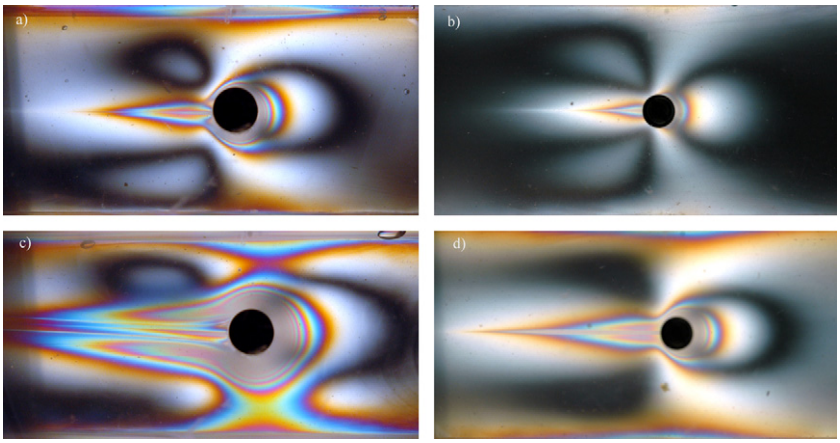

Fig. 6. The extensional birefringent patterns produced by setting the crossed polarizers at 45° and 135° for the CTAB/NaSal solution at blockage ratios of 1:10 (right) and 1:5 (left) at Deborah numbers of $De = 2$ (a and b) and $De = 4$ (c and d). The flow is from right to left.

than the CTAB/NaSal as evidenced by the fringe gradients seen in Fig. 5.

The relative contribution of shear and confinement is made clear by comparing the birefringent patterns produced by the CTAB/NaSal solution at the two different blockage ratios seen in Fig. 6. If the length and width of the extensional birefringent tail are normalized by the diameter of the cylinder, l/D or w/D, they are found to scale with the Deborah number. If instead the birefringence measurements from the crossed polarizers oriented at 0° and 90° were shown for both blockage ratios, one would observe that the shear deformation along the walls scales with the Weissenberg number instead of the Deborah number. Thus for the 1:10 blockage ratio, deformation due to shear is far less significant than it is for the 1:5 blockage ratio at the same Deborah numbers. More importantly, these images also demonstrate that direct interaction between the shear flow and the extensional flow in the wake of the cylinder is not required for the flow to become unstable.

The birefringent tail present in the CTAB/NaSal solution grows in both the spanwise and flow directions until the flow becomes unstable at a Deborah number of roughly $De = 4.5$ for the 1:5 blockage ratio and roughly $De = 6$ in the case of the 1:10 blockage ratio. As such, the images above this Deborah number presented in Fig. 6 are valid only for an instant in time chosen to be the point in time just prior to the onset of the elastic instability. This instant is chosen so that the largest values of stress the material can support are compared in a direct manner. In order to gain a better understanding of the behavior of these patterns a time series of exposures is necessary. Presented in Fig. 7 is a sample of the time-dependant birefringent patterns produced by the CTAB/NaSal solution. As the flow develops from startup, the fringe gradients in the extensional tail increase, indicating a building of deformation and stress. At some critical stress, the fluid appears to tear in the wake of the cylinder. The result is a sudden acceleration of the fluid, a break in the vertical symmetry, and a reduction in the number of fringes and thus the extensional deformation and stress in the fluid. This observation is more easily seen from images taken looking down on the cylinder in the gradient direction as seen in Fig. 8. As seen in Fig. 8, the instability initiates at a random location near the aft stagnation point of the cylinder. The FIB shows an apparent rupture of the wormlike micelle solutions which appears as a sudden reduction of the extensional stress. This instability appears similar to that observed during other extensional flows of wormlike micelle solutions [21,30,32,33,43]. This rupture event propagates axially along the cylinder a short distance initially about one cylinder diameter before stopping. As the Deborah number is increased, the rupture events occur more frequently and propagate further along the cylinder. As discussed in the previous section, the rupture events appear to be chaotic in nature. No dominant frequency can be observed even at Deborah numbers just beyond the critical conditions. Further, evidence of this instability can be seen in Fig. 8 as a striation in the birefringence tail in wake of the cylinder. The form of the instability is very different from that observed experimentally for viscoelastic polymer solutions. In those experiments, a series of stationary counter-rotating vortices were observed in the wake of the cylinder [3,9]. Additionally, for polymer solutions, the vortices in the wake of the cylinder has been shown to have no effect on the flow upstream of the cylinder [9], while in our experiments, the rupture events are found to propagate both downstream and upstream of the cylinder affecting the flow everywhere in the channel. A similar tearing instability was observed by Gladden and Belmonte [44] who pulled a series of different cylinder shapes through a shallow layer of viscoelastic wormlike micelle solutions.

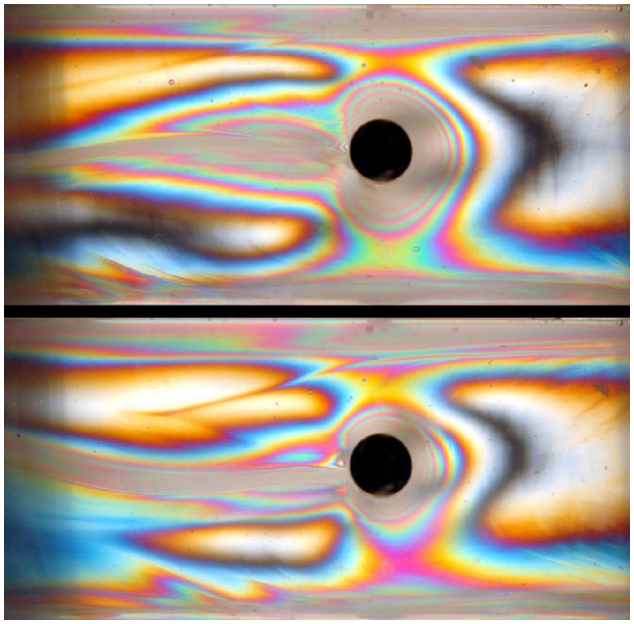

Fig. 7. Time sequence of the extensional birefringence of the CTAB/NaSal solution. As the fluid flows from right to left, the extensional tail in the wake of the cylinder grows until rupture and the fluid accelerates. Here the time difference between the two images is 2 s or roughly two periods of the instability. The flow is from right to left.

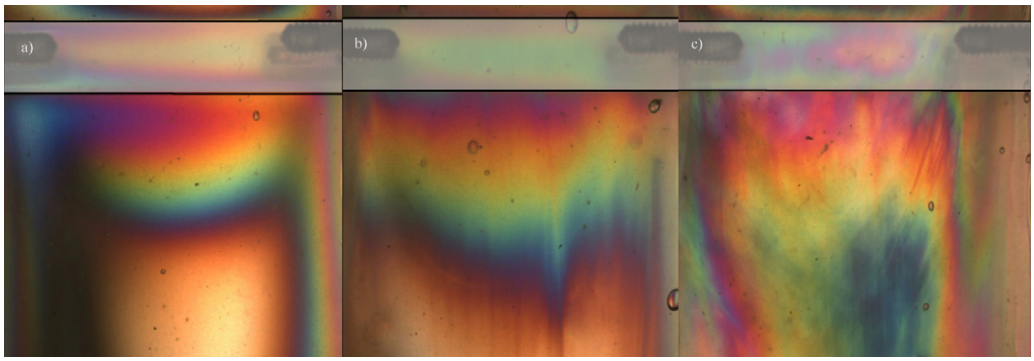

Fig. 8. Flow-induced birefringent measurements of the *xz*-plane with crossed polarizers aligned at 45° and 135° to isolate the extensional stress. The fluid is the CTAB/NaSal solution at blockage ratios of 1:10 at (a) Deborah numbers of $De = 8$ during startup prior to the onset of the instability, (b) $De = 8$ after several rupture events, and (c) $De = 16$ after a great many rupture events. The flow is from top to bottom.

3.3. Particle image velocimetry (PIV)

Particle image velocimetry (PIV) was employed to create full-field velocity fields for both of the test fluids and blockage ratios over the entire range of Deborah numbers probed. Details of the PIV setup and procedures used in these experiments can be found in Moss and Rothstein [45]. While full vector fields allow for a clear quantitative picture of the flow fields at any instant in time, it is most instructive to examine 'slices' of the vector field so that the evolution of the flow field can be more easily ascertained. By taking a number of slices through the vector field along the flow direction it is possible to track the evolution of the velocity profiles as the fluid flows past the cylinder. Such a representative series of profiles are presented in Fig. 9. As the fluid progresses towards the cylinder, the profiles depart from the flattened parabola characteristic of shear thinning fluid to become two distinct flattened parabolas enclosing the circular cylinder. The impact of the cylinder can be seen in the velocity profiles as far as ten radii downstream of the cylinder before the parabolic flow is re-achieved. These profiles clearly show the effect of the cylinder on the flow kinematics and closely resemble both the experimental and numerical literature for the flow of polymer solution [3,4,10,12,20,46].

In Fig. 10a, the centerline velocity profiles for the CPyCl/NaSal solution are presented as a function of distance in the flow direction so that the extensional flow in the wake of the cylinder and the deviation from Newtonian flow can be quantified. Here, the x-component of the velocity is normalized by the mass-averaged mean stream velocity, v_x/U. As before, such calculations have been performed for all test solutions and blockage ratios studied, but only a representative subset is presented in the interest of space and clarity. The trends in the CTAB/NaSal solution mirrored the CPyCl/NaSal solution, however, good PIV could only be captured up to the point that the flow became unstable at $De = 4.5$. For this reason the CPyCl/NaSal solutions were chosen for Fig. 10 so that results up to $De = 8$ could be presented. For both test fluids, the velocity begins at zero at the aft stagnation point of the cylinder and increases to the expected centerline velocity far from the cylinder. For a shear thinning fluid like the CPyCl/NaSal solution which has a power-law exponent of approximately $n \approx 1/3$ over the range of Deborah numbers studied, a centerline velocity of approximately $v_x/U \approx 1.25$ [38]. As has been observed in the previous literature [3,10,15,40], the velocity returns to the unperturbed channel flow solution more slowly with increasing Deborah number indicating an increase in strength and extent of the extensional flow in the wake of the cylinder.

The velocity profiles in Fig. 10a can be used to calculate the local values of the extension rate and accumulated strain in the wake of the cylinder. These calculations can be compared directly to the

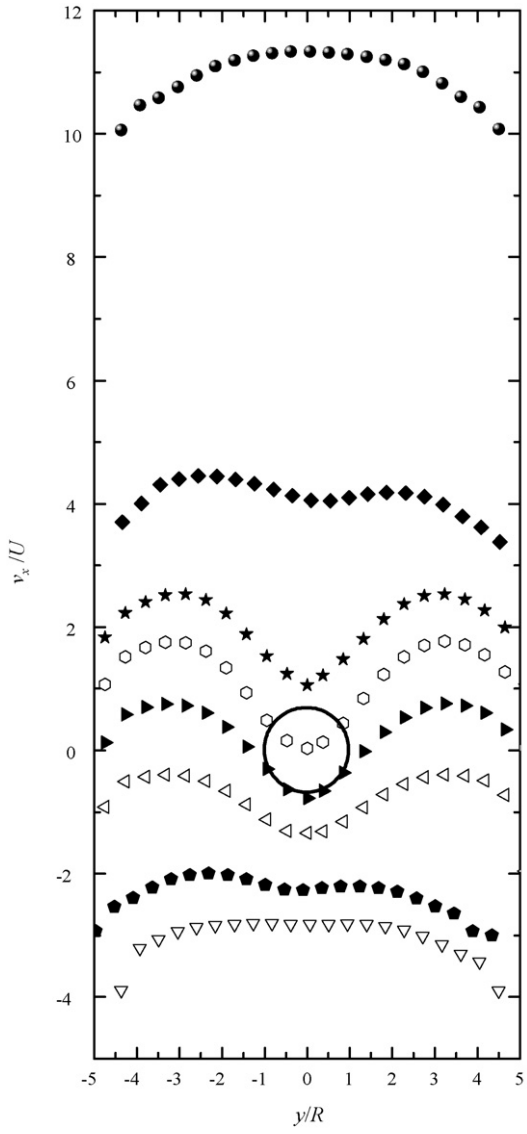

Fig. 9. Non-dimensional velocity profiles for multiple positions along the flow direction. The effect of the cylinder can clearly be seen. The vectors are calculated for the CPyCl/NaSal solution at a Deborah number of $De = 0.5$.

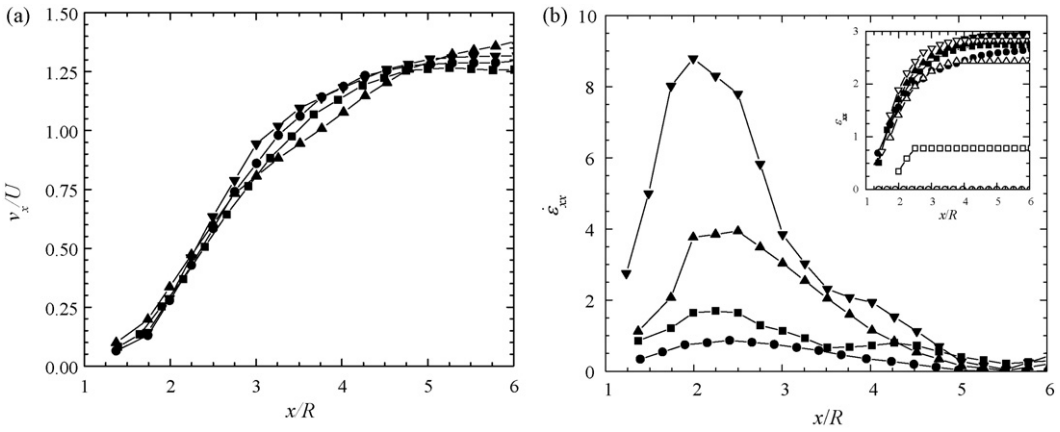

Fig. 10. Normalized centerline velocity profiles (a) along with the resulting extension rate (b) and accumulated strain (inset b) for the CPyCl/NaSal solution as a function of non-dimensional downstream distance in the 1:5 blockage ratio channel. Shown are curves of Deborah number $De = 0.5$ (■), $De = 2$ (●), $De = 4$ (▲), and $De = 8$ (▼). The hollow symbols in the inset of (b) correspond to the fraction of the total strain accumulated from regions in the flow where the local Deborah number exceeds $De_{ext} > 0.5$.

extensional rheology measurements presented in Fig. 2 to determine if the instability can be correlated to the filament rupture in those experiments. The extension rate in the wake of the cylinder is given by

$$\dot{\varepsilon}_{xx} = \frac{\partial v_x}{\partial x}, \tag{2}$$

and is tabulated for CPyCl/NaSal solutions in Fig. 10b for the velocity profiles presented in Fig. 10a. Additionally, the total strain can be calculated by integrating the extension rate in the wake of the cylinder:

$$\varepsilon_{xx} = \int \frac{\partial v_x}{\partial x}\, dt = \int \frac{dv_x}{v_x}, \tag{3}$$

which is given in the inset of Fig. 10b. The local extension rate can in turn be used to calculate a local value of the Deborah number for the extensional flow in the wake of the cylinder, $De_{ext} = \lambda\dot{\varepsilon}_{xx}$. With the equivalent Deborah number in hand, the extensional rheological data can be used to gain insight into the nature of the flow and the flow instability. In the case of the CPyCl/NaSal solutions, the maximum extension rate in the wake of the cylinder ranged from $\dot{\varepsilon} = 0.50\,s^{-1}$ ($De_{ext} = 0.25$) to $\dot{\varepsilon} = 8.8\,s^{-1}$ ($De_{ext} = 4.4$) at a bulk Deborah number of $De = 0.5$ and $De = 8$ as shown in Fig. 10b. For the CTAB/NaSal solutions, the maximum extension rate ranged from $\dot{\varepsilon} = 0.12\,s^{-1}$ ($De_{ext} = 0.68$) at $De = 0.5$ to a value of $\dot{\varepsilon} = 0.9\,s^{-1}$ ($De_{ext} = 5.1$) at $De = 4$. In all cases, the extension rate initially increases quickly downstream of the cylinder before it reaches a maximum and eventually approaches zero at a distance of five or more radii downstream. At higher Deborah numbers, the maximum extension rate moves progressively upstream, closer to the cylinder even as the extensional flow is found to extend further downstream of the cylinder. These measurements are consistent for both surfactant solutions tested and are in good qualitative agreement with both experimental measurements and numerical simulations for the flow of polymer solutions past circular cylinders [3]. As the solid symbols in the inset of Fig. 10b demonstrate, the total accumulated strain calculated by integrated equation (3) from the location of the first PIV velocity vector downstream of the cylinder remains nearly constant at a value of approximately $\varepsilon \approx 2.8$. This was consistent for the CPyCl/NaSal solution at all of the Deborah numbers tested, but it was also true for the CTAB/NaSal solution at both blockage ratios tested. However, it is important to note that even as the total strain remains nearly independent of flow rate, much of this strain, especially at lower flow rates, is accumulated at extension rates for which the local Deborah number is well below one and the micelles are not significantly deformed. A better measure might be to plot the fraction of the total strain accumulated in regions of the flow where the local Deborah number is greater than $De_{ext} > 0.5$. These effective strain data are shown in Fig. 10b as hollow symbols in the inset and demonstrate an increase in effective strain with increasing Deborah number which is consistent with the birefringence measurements.

For the CTAB/NaSal solutions at the critical Deborah numbers for the onset of the elastic instability ($De = 4.5$ in the case of the 1:5 blockage ratio, and $De = 6$ in the case of the 1:10 blockage ratio), the PIV data show local Deborah numbers greater than $De_{ext} > 0.5$ and effective strains that are greater than $\varepsilon > 2.5$. For the CTAB/NaSal solutions, this extensional flow is strong enough to induce a rupture event in the filament stretching experiments presented in Fig. 2 and the elastic instability observed in the wake of the cylinder. However, for flows of the CPyCl/NaSal solutions even at the largest Deborah numbers that could be probed, effective strains greater than $\varepsilon > 3.3$ were not achieved. As seen in Fig. 2, this strain is needed to cause a CPyCl/NaSal solution filament to fail in a pure extensional flow. The difference in stability of these two solutions as the flow past a confined circular cylinder thus appears to be directly related to their extensional rheology and their stability in purely extensional flows. Finally, if this were the purely elastic flow instability previously observed for polymer solutions flowing past a single cylinder one would expect both fluids to become unstable at roughly the same Deborah number independent of fluid composition [10,12,14,16,20,25,44].

4. Conclusions

In this work, the results of an investigation into the flow fields generated by two different solutions of wormlike micelles in cross-flow past a single circular cylinder of two blockage ratios. Although this benchmark flow has been studied in great detail in the past using viscoelastic polymer solutions, these experiments are the first to use a viscoelastic wormlike micelle solution as the test fluid. The role fluid rheology and blockage ratio were investigated by systematically varying the Deborah number and measuring the flow kinematics, stability and pressure drop. In both blockage ratios, the normalized pressure drop was found to initially decrease due to the shear thinning of the test fluid, before reaching a plateau as extensional effects begin to dominate the flow. An elastic instability in one of the test fluids, CTAB/NaSal, was observed above a critical Deborah number, while the other fluid, CPyCl/NaSal, was found to remain stable over all flow rates tested. The kinematics of both fluids was fully investigated using PIV and FIB to elucidate the nature

of the flow and the observed elastic instability in the case of the CTAB/NaSal solution.

At low Deborah numbers, both fluids exhibit similar responses: symmetric streamlines, and the normalized pressure drop remains constant with increasing Deborah number. At moderate Deborah numbers, where the response is dominated by shear thinning, the normalized pressure drop measurements were found to decay with increasing Deborah number for both fluids and velocity profiles of the two fluids demonstrated similar trends. However, the flow-induced birefringence patterns reveal that at comparable Deborah numbers, the two fluids show disparate degrees of micellar configurational changes with the CTAB/NaSal becoming much more highly birefringent in the wake of the cylinder. This is a direct result of the significant differences in the fluids' extensional rheology. At comparable Deborah numbers, the CTAB/NaSal solution strain hardens much more quickly than the CPyCl/NaSal. At even higher Deborah numbers, the extensional rheology begins to become increasingly important to the response of the fluids as the birefringent wake is observed to extend far downstream of the cylinder. In this region, the normalized pressure drop, which initially decreased due to the shear thinning caused by the bounding walls of the flow cell, was observed to level off as extensional effect begin to dominate.

At a Deborah number of $De = 4.5$ for the 1:5 blockage ratio and $De = 6.0$ for the 1:10 blockage ratio, the CTAB/NaSal solution was found to become unstable while the CPyCl/NaSal solution remained stable for all the Deborah numbers tested. Because the critical Deborah number was observed to be only weakly dependent on the blockage ratio these measurements clearly indicate that the instability is related not to the shear flow, but the extensional flow in the wake of the cylinder. Perhaps more importantly, the FIB images show that direct interaction between the shear flow along the walls of flow cell and the extensional flow in the wake of the cylinder is not required for the flow to become unstable. This is an observation that could not be made when studying the flow through a periodic array of cylinders were a similar flow instability was observed [21].

PIV measurements were used to further probe the strength of the extensional flow in the wake of the cylinder by calculating both an extension rate and accumulated strain from the velocity profile. In all cases, the extension rate was found to initially increases quickly downstream of the cylinder before it reaches a maximum and eventually approaches zero several diameters downstream of the cylinder. At higher Deborah numbers, the maximum extension rate moves progressively upstream, closer to the cylinder even as the extensional flow was found to extend further downstream of the cylinder. The total strain accumulated at an extensional Deborah number above $De_{ext} > 0.5$ was found to increase with increasing flow rate, however, the total strain was never found to grew larger than $\varepsilon = 3.0$. If one examines the extensional rheology of the two test fluids, a dramatic rupture of the fluid filament is observed for both fluids after significant strain hardening has been achieved in the filament stretching experiment. However, at the extension rates and strains accumulated by the micelle solutions in the wake of a single cylinder, the extensional rheology of these fluids suggests that only the CTAB/NaSal solution would be expected to become unstable. The effective strain accumulated by the CPyCl/NaSal solution is simply not enough to cause the solution of wormlike micelles to fail *en masse*.

Acknowledgements

The authors would like to acknowledge the National Science Foundation for financial support of this research under grant CBET-0547150 and the MRSEC at the University of Massachusetts at Amherst for use of its shear rheometer.

References

[1] G.H. McKinley, Steady and transient motion of spherical particles in viscoelastic liquids, in: R. Chhabra, D. De Kee (Eds.), Transport Processes in Bubbles, Drops & Particles, Taylor and Francis, New York, 2001.
[2] K. Walters, R.I. Tanner, The motion of a sphere through an elastic liquid, in: R. Chhabra, D. De Kee (Eds.), Transport Processes in Bubbles, Drops and Particles, Hemisphere Publ. Corp., New York, 1992.
[3] G.H. McKinley, R.C. Armstrong, R.A. Brown, The wake instability in viscoelastic flow past confined cylinders, Philos. Trans. R. Soc. Lond. A 344 (1993) 265–304.
[4] A.H. Shiang, J.C. Lin, A. Oztekin, D. Rockwell, Viscoelastic flow around a confined circular cylinder: measurements using high-image-density particle image velocimetry, J. Non-Newtonian Fluid Mech. 73 (1997) 29–49.
[5] L. Bairstow, B.M. Cave, E.D. Lang, The resistance of a cylinder moving in a viscous fluid, Philos. Trans. R. Soc. Lond. A 223 (1923) 383–432.
[6] H. Lamb, Hydrodynamics, Dover, New York, 1945.
[7] M.D. Chilcott, J.M. Rallison, Creeping flow of dilute polymer-solutions past cylinders and spheres, J. Non-Newtonian Fluid Mech. 29 (1988) 381–432.
[8] R.G. Larson, Instabilities in viscoelastic flows, Rheol. Acta 31 (1992) 213–263.
[9] A.H. Shiang, A. Oztekin, J.C. Lin, D. Rockwell, Hydroelastic instabilities in viscoelastic flow past a cylinder confined in a channel, Exp. Fluids 28 (2000) 128–142.
[10] H.P.W. Baaijens, G.W.M. Peters, F.P.T. Baaijens, H.E.H. Meijer, Viscoelastic flow past a confined cylinder of a polyisobutylene solution, J. Rheol. 39 (1995) 1243–1277.
[11] J. Chakraborty, N. Verma, R.P. Chhabra, Wall effects in flow past a circular cylinder in a plane channel: a numerical study, Chem. Eng. Proc. 43 (2004) 1529–1537.
[12] S.A. Dhahir, K. Walters, On non-Newtonian flow past a cylinder in a confined flow, J. Rheol. 33 (1989) 781–804.
[13] P.Y. Huang, J. Feng, Wall effects on the flow of viscoelastic fluids around a circular-cylinder, J. Non-Newtonian Fluid Mech. 60 (1995) 179–198.
[14] M.A. Hulsen, R. Fattal, R. Kupferman, Flow of viscoelastic fluids past a cylinder at high Weissenberg number: stabilized simulations using matrix logarithms, J. Non-Newtonian Fluid Mech. 127 (2005) 27–39.
[15] J.M. Kim, C. Kim, C. Chung, K.H. Ahn, S.J. Lee, Negative wake generation of FENE-CR fluids in uniform and Poiseuille flows past a cylinder, Rheol. Acta 44 (2005) 600–613.
[16] O. Manero, B. Mena, On the slow flow of viscoelastic liquids past a circular-cylinder, J. Non-Newtonian Fluid Mech. 9 (1981) 379–387.
[17] H. Usui, T. Shibata, Y. Sano, Karman vortex behind a circular-cylinder in dilute polymer-solutions, J. Chem. Eng. Japan 13 (1980) 77–79.
[18] J.P. Rothstein, G.H. McKinley, The axisymmetric contraction–expansion: the role of extensional rheology on vortex growth dynamics and the enhanced pressure drop, J. Non-Newtonian Fluid Mech. 98 (2001) 33–63.
[19] P.J. Oliveira, A.I.P. Miranda, A numerical study of steady and unsteady viscoelastic flow past bounded cylinders, J. Non-Newtonian Fluid Mech. 127 (2005) 51–66.
[20] F.P.T. Baaijens, S.H.A. Selen, H.P.W. Baaijens, G.W.M. Peters, H.E.H. Meijer, Viscoelastic flow past a confined cylinder of a low density polyethylene melt, J. Non-Newtonian Fluid Mech. 68 (1997) 173–203.
[21] G.R. Moss, J.P. Rothstein, Flow of viscoelastic wormlike micelle solutions through a periodic array of cylinders, J. Non-Newtonian Fluid Mech. 165 (2009) 1–13.
[22] J.N. Israelachvili, Intermolecular and Surface Forces: With Applications to Colloidal and Biological Systems, Academic Press, London, 1985.
[23] R.G. Larson, The Structure, Rheology of Complex Fluids, Oxford University Press, New York, 1999.
[24] H. Rehage, H. Hoffmann, Viscoelastic surfactant solutions: model systems for rheological research, Mol. Phys. 74 (1991) 933–973.
[25] S. Ogata, Y. Osano, K. Watanabe, Effect of surfactant solutions on the drag and the flow pattern of a circular cylinder, AIChE J. 52 (2006) 49–57.
[26] C. Bergins, M. Nowak, M. Urban, The flow of a dilute cationic surfactant solution past a circular cylinder, Exp. Fluids 30 (2001) 410–417.
[27] J.L. Zakin, H.W. Bewersdorff, Surfactant drag reduction, Rev. Chem. Eng. 14 (1998) 253–320.
[28] R.G. Laughlin, The Aqueous Phase Behavior of Surfactants, Academic Press, New York, 1994.
[29] J. Appell, G. Porte, A. Khatory, F. Kern, S.J. Candau, Static and dynamic properties of a network of wormlike surfactant micelles (etylpyridinium chlorate in sodium chlorate brine), J. Phys. II 2 (1992) 1045–1052.
[30] J.P. Rothstein, Transient extensional rheology of wormlike micelle solutions, J. Rheol. 47 (2003) 1227–1247.
[31] S.M. Fielding, Complex dynamics of shear banded flows, Soft Matter 3 (2007) 1262–1279.
[32] A. Bhardwaj, E. Miller, J.P. Rothstein, Filament stretching and capillary breakup extensional rheometry measurements of viscoelastic wormlike micelle solutions, J. Rheol. 51 (2007) 693–719.
[33] S. Chen, J.P. Rothstein, Flow of a wormlike micelle solution past a falling sphere, J. Non-Newtonian Fluid Mech. 116 (2004) 205–234.
[34] A. Jayaraman, A. Belmonte, Oscillations of a solid sphere falling through a wormlike micelle solution, Phys. Rev. E 67 (2003) 065301–65304.
[35] E. Miller, J.P. Rothstein, Transient evolution of shear banding in wormlike micelle solutions, J. Non-Newtonian Fluid Mech. 143 (2007) 22–37.

[36] A. Bhardwaj, D. Richter, M. Chellamuthu, J.P. Rothstein, The effect of preshear on the extensional rheology of wormlike micelle solutions, Rheol. Acta 46 (2007) 861–875.
[37] L.M. Walker, P. Moldenaers, J.-F. Berret, Macroscopic response of wormlike micelles to elongational flow, Langmuir 12 (1996) 6309–6314.
[38] R.B. Bird, R.C. Armstrong, O. Hassager, Dynamics of Polymeric Liquids: Volume 1 Fluid Mechanics, John Wiley & Sons, New York, 1987.
[39] J.M. Verhelst, F.T.M. Nieuwstadt, Visco-elastic flow past circular cylinders mounted in a channel: experimental measurements of velocity and drag, J. Non-Newtonian Fluid Mech. 116 (2004) 301–328.
[40] A. Afonso, M.A. Alves, F.T. Pinho, P.J. Oliveira, Uniform flow of viscoelastic fluids past a confined falling cylinder, Rheol. Acta 47 (2008) 325–348.
[41] R. Cressely, R. Hocquart, Localized flow birefringence induced in the wake of obstackles, Opt. Acta 27 (1980) 699–711.
[42] C. Chen, G.G. Warr, Light scattering from wormlike micelles in an elongational flow, Langmuir 13 (1997) 1374–1376.
[43] J.P. Rothstein, Strong flows of viscoelastic wormlike micelle solutions, in: D.M. Binding, K. Walters (Eds.), Rheology Reviews, The British Society of Rheology, Aberystwyth, Wales, UK, 2008.
[44] J.R. Gladden, A. Belmonte, Motion of a viscoelastic micellar fluid around a cylinder: flow and fracture, Phys. Rev. Lett. 98 (2007) 224501.
[45] G.R. Moss, J.P. Rothstein, Flow of viscoelastic wormlike micelle solutions through a periodic array of cylinders, J. Non-Newtonian Fluid Mech. 165 (2010) 1–13.
[46] R.P. Chhabra, A.A. Soares, J.M. Ferreira, Steady non-Newtonian flow past a circular cylinder: a numerical study, Acta Mech. 172 (2004) 1–16.